A dinuclear dysprosium Schiff base complex showing slow magnetic relaxation in the absence of an external magnetic field†

Mamo Gebrezgiabher, [ID] [ab] Sören Schlittenhardt, [ID] [c] Cyril Rajnák, [ID] [b]
Juraj Kuchár, [ID] [d] Assefa Sergawie, [a] Juraj Černák, [ID] [d] Mario Ruben, *[cef]
Madhu Thomas [ID] *[a] and Roman Boča [ID] [b]

A dinuclear dysprosium(III) complex $[Dy_2(NO_3)_3(L)_3] \cdot n CH_3OH$ (n = 1.20; HL = (2-[(2-hydroxy-propylimino)-methyl]phenol)) (**1**) was isolated when dysprosium nitrate reacted with a solution of salicylaldehyde and 1-amino-2-propanol in a basic medium under *in-situ* reaction conditions. The isolated complex was characterized by single crystal X-ray diffraction studies at room temperature. The complex is built up of a dinuclear {Dy_2} molecule in which the two Dy(III) central atoms are triply linked by O-monoatomic bridges arising from deprotonated hydroxyl groups of the three L ligands; these act as doubly chelating & bridging ligands. Both Dy(III) atoms exhibit nona-coordination with donor sets O_8N and O_7N_2, respectively. The coordination spheres of the respective Dy(III) atoms are completed by one or two chelating nitrato ligands. The magnetic properties of **1** have been investigated by DC and AC susceptibility measurements. The DC measurements reveal a slight exchange coupling of an antiferromagnetic nature. The out-of-phase AC susceptibility signal is seen even at zero applied field. The low-frequency relaxation mode is supported by an external magnetic field.

Introduction

Single-molecule magnets (SMMs) are usually coordination compounds, showing superparamagnetic nature below a certain blocking temperature at the molecular level and having diverse applications in high density information storage, quantum computing and molecular spintronics.[1-3] This interdisciplinary

[a] *Department of Industrial Chemistry, College of Applied Sciences, Nanotechnology Excellence Center, Addis Ababa Science and Technology University, Addis Ababa P.O. Box 16417, Ethiopia. E-mail: madhu.thomas@aastu.edu.et*

[b] *Department of Chemistry, Faculty of Natural Sciences, University of SS Cyril and Methodius, 91701 Trnava, Slovakia*
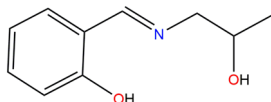
[c] *Institute of Nanotechnology, Karlsruhe Institute of Technology, Hermann-von-Helmholtz-Platz 1, 76344 Eggenstein-Leopoldshafen, Germany. E-mail: mario.ruben@kit.edu*

[d] *Department of Inorganic Chemistry, Institute of Chemistry, P. J. Šafárik University in Košice, Moyzesova 11, 041 54 Košice, Slovakia*

[e] *Institute of Quantum Materials and Technologies (IQMT), Karlsruhe Institute of Technology, Hermann-von-Helmholtz-Platz 1, 76344 Eggenstein-Leopoldshafen, Germany*

[f] *Centre Européen de Science Quantique (CESQ), Institut de Science et d'Ingénierie Supramoléculaires (ISIS, UMR 7006), CNRS-Université de Strasbourg, 8 allée Gaspard Monge BP 70028 67083 Strasbourg Cedex, France*

† Electronic supplementary information (ESI) available: X-ray structure analysis, and crystallographic and physical data. CCDC 2122185.

field of molecular magnetism has undergone revolutionary changes since the early 1990's.[4] In continuation of the very first dodecanuclear manganese SMM,[5] there have been ample homometallic[6-10] and heterometallic[11-18] transition metal SMMs reported in the literature to date. Lanthanide based SMMs have received special attention in this area on account of their large spin state and high magnetic anisotropy.[1,2,19-23] Ever since the discovery of the exotic Dy_3 by Powell *et al.*[24] and because of its large magnetic moment and high anisotropy, Dy(III) based SMMs have drawn the attention of many investigators.[25-37] The significance of Dy-SMM chemistry is very remarkable as evident from the discovery of dinuclear[38] and pentanuclear[39] aggregates with a high energy barrier for the reversal of magnetization.

It has been revealed in the previous studies[40,41] that the ligand field and the coordination geometry generally have a pronounced effect on the magnetization dynamics. In this context, Schiff bases are ideal candidates because of their fine tunability for the ligand field by varying the substituents of both aldehydic and amine precursors.[31,42,43]

This fact is supported by the large number of reports on constructing lanthanide-based SMMs[25-37] especially those based on dysprosium[19,31,34,44] and Schiff bases, which can be effectively employed in constructing SMMs with desired properties.

Herein, we report our investigations on the single crystal structure at room temperature and field dependent magnetic

Scheme 1 The Schiff base ligand (H$_2$L) from salicylaldehyde and 1-amino-2-propanol.

properties on the methanol solvate of the dinuclear dysprosium(III) complex [Dy$_2$(NO$_3$)$_3$(L)$_3$]·nCH$_3$OH with L being a deprotonated Schiff base derived from salicylaldehyde and 1-amino-2-propanol (Scheme 1), synthesised by an *in-situ* method.

Experimental section

General procedures

All starting materials such as dysprosium nitrate hexahydrate, salicylaldehyde, 1-amino-2-propanol, triethylamine and methanol were of analytical reagent grade and were used as commercially obtained without further purification. For preparing the complex, the lanthanide salt was added dropwise to a stirring solution of salicylaldehyde with 1-amino-2-propanol and triethylamine in a 1:1 ratio in methanol. Elemental analysis for C, H, and N was carried out on Flash 2000 CHNSO apparatus (Thermo Scientific). FTIR spectra were measured in the region 400–4000 cm^{-1} at room temperature (Shimadzu IR Affinity $^{-1}$).

Magnetic susceptibility data were collected at temperatures between 2–300 K using a Quantum Design MPMS-XL SQUID magnetometer equipped with a 5 T magnet at an external field of 0.1 T. The samples were ground and fixed in a gelatine capsule using small amounts of eicosane to avoid any movement of the sample. The experimental magnetic susceptibility data were corrected for the underlying diamagnetism.

Synthesis of dinuclear dysprosium Schiff base complex (1)

A solution of Dy(NO$_3$)·6H$_2$O (1 mmol, 0.348 g) in 15 mL methanol was added dropwise to a stirred methanolic solution of salicylaldehyde (1 mmol, 0.122 mL) and 1-amino-2-propanol (1 mmol, 0.075 mL) in the presence of triethylamine (1 mmol, 0.101 mL) (50 mL). The resultant mixture was refluxed for 4 hours in an oil bath, cooled and filtered. Vapour diffusion of diethyl ether to the filtrate yielded yellow blocks of crystals suitable for X-ray diffraction. The complex was collected by filtration and washed with cold MeOH and dried in air and vacuum. Yield: 180 mg/33% Anal. calcd for complex **1**, C$_{30}$H$_{36}$Dy$_2$N$_6$O$_{15}$ + 1.2 methanol (Mr = 1082.86) (Scheme 2): C,
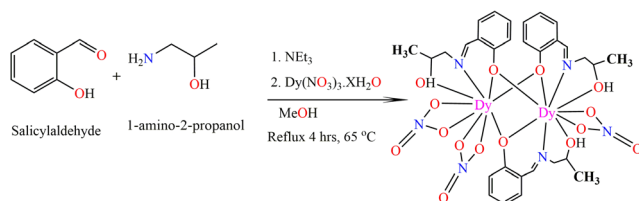
Scheme 2 Schematic representation of the reaction procedure to obtain complex **1**.

34.54%; H, 3.65%; N, 7.75%. Found: C, 34.47%; H, 3.49%; N, 7.63%. IR (KBr disc)/cm^{-1}: 3389(Br), 1635(s), 1588(m), 1551(m), 1468(w), 1431(w),1281(s), 1135 (m), 1027(s), 892(m), 772(s), 659(s), 607(m), 412 (m).

X-ray crystallography

X-ray diffraction measurements were taken at 299.15 K on a Gemini diffractometer (Rigaku-OD) with an Atlas S2 CCD detector with graphite-monochromated Mo Kα radiation (λ = 0.71073 Å). The data collection was done using the CrysAllisPro system.[45] The data were corrected for absorption using numerical absorption correction based on Gaussian integration over a multifaceted crystal model, with T_{min} = 0.520 and T_{max} = 0.623. The structure of the compound was solved by direct methods and refined by full-matrix least-squares techniques on F^2 using program SHELXT,[46–48] which was incorporated in the WinGX program package.[49] All non-hydrogen atoms including the well-defined methanol solvate molecule were refined with anisotropic thermal parameters. Hydrogen atoms on the Schiff base-type ligands were placed in the calculated positions and allowed to ride on the parent atoms with isotropic thermal parameters tied with the parent atoms (U(H) = 1.2U(CH$_2$) and U(H) = 1.5U(CH$_3$)), but the positional coordinates of the methine (C)–H hydrogen atoms were freely refined while the positional coordinates of the hydroxyl hydrogen atoms within the ligand and in the methanol (C41, O41 atoms) solvate molecule were refined with application of restrained O–H distances. The site occupation factor of the well-defined methanol molecule was refined and its value converged to 0.870(7). The packing mode of the dinuclear complex molecules leads to the formation of channels running along the −3 axis. In the difference map were found small maxima positioned on this axis and these were interpreted as additional disordered methanol solvate molecules with half occupancies due to the closeness of their positions. Due to the disorder and very high thermal motion, these atoms were included in the model with isotropic thermal parameters and no attempt was made to localize the hydrogen atoms of these molecules. Structural figures were drawn using the Diamond program.[50] Crystal data and refinement results for the complex are summarized in Table S1 (ESI†) and the selected bond lengths and bond angles of the complex are presented in Table S2 (ESI†).

Results and discussion

The dinuclear dysprosium complex **1** was isolated by reacting hydrated dysprosium nitrate with salicylaldehyde and 1-amino-2-propanol in the presence of triethylamine in a methanolic medium under *in situ* conditions. The Schiff base ligand is chelated to each metal center in a tridentate fashion (Scheme 2 and Fig. 1). The dinuclear complex **1** was crystallized from the reaction mixture by vapor diffusion of diethyl ether. A somewhat similar structural motif like that of **1** has been reported by Zhang *et al.* at 186 K.[51] In addition, they have studied the luminescence properties of the dinuclear aggregates.
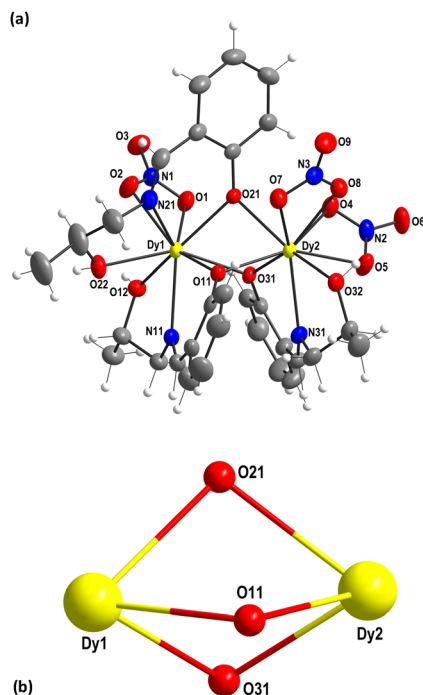
Fig. 1 (a) Thermal ellipsoid plot of the dinuclear complex molecule in **1**. The carbon and hydrogen atoms are not labelled for clarity. The thermal ellipsoids are drawn at the 30% probability level; (b) the dinuclear {Dy$_2$} core in **1**.

Our compound was isolated under *in situ* conditions in comparison with Zhang's compound, which was prepared from a prepared Schiff base ligand. In the present study, we have created flexible reaction conditions by which the metal can bind to a variety of coordinating ligands in addition to the Schiff base, such as precursors, solvents *etc.*

In the infrared spectra of complex **1**, the intense band at 1635 cm^{-1} is assigned to the azomethine groups, ν(C N). The broad band around 3375 cm^{-1} is assigned to the O–H vibrations of the aliphatic alcoholic portion in the ligand. The stretching frequencies at about 1135 cm^{-1} for the complex are attributed to the coordinated C–O of ring phenolic oxygen (Fig S1, ESI†).[52]

Structural description of 1

The crystal structure of **1** had already been studied at 186 K (PICBUA) along with some other isostructural Ln(III) complexes, but the detailed structural description was not given in that study.[51] As we have decided to study the magnetic properties of the title complex **1**, we have redetermined its crystal structure at RT and here we briefly describe the molecular and supramolecular structure of **1**, which is relevant with respect to the studied magnetic properties. A look in Table S1 (ESI†) shows that the unit cell volume of complex **1** at RT is higher (18858.4(12) Å) than the one measured at 186 K (18713.5(1) Å) and this is what was expected due to different temperatures of the X-ray experiments. We note also different contents of methanol solvent molecules at RT and 186 K (PICBUA) as we

have found additional highly disordered methanol solvent molecules in the formed canals (see below). The crystal structure of **1** is built up of dinuclear complex molecules in which two Dy(III) atoms are linked by three deprotonated Schiff base-type ligands L (Fig. 1). The distance between the two Dy(III) atoms is rather short, 3.4552(2) Å and 3.454 Å at 186 K.[51] Similar closeness of two Dy(III) atoms (3.485 Å) in dinuclear triply O-bridged complexes was already observed, *e.g.* in [Dy$_2$(*quin*)$_4$(NO$_3$)$_3$]·H$_2$*quin*· CH$_3$OH (H*quin* = 8-hydroxyquinoline).[53] Such close arrangement of two Dy(III) atoms may be important from a magnetic properties point of view as it may lead to magnetic exchange interactions between them.

The three crystallographically independent Schiff base ligands L act as tridentate ligands forming two chelate rings with one Dy(III) central atom and, at the same time, it acts as a bridging ligand linking the two Dy1 and Dy2 atoms by phenoxido O-monoatomic bridges (O11, O21 and O31) (Fig. 1). The corresponding Dy–O–Dy angles are 95.64(1)°, 95.63(1)° and 95.74(1)° for Dy1–O11–Dy, Dy1–O21–Dy2 and Dy1–O31–Dy2, respectively (Fig. 1b). The bridging atoms O11, O21 and O31 form an approximate isosceles triangle with O11···O21, O11···O31 and O21···O31 distances of 2.697(5) Å, 2.799(4) Å and 2.625(3) Å, respectively. These values are slightly smaller than those reported in similar other lanthanide dinuclear complexes[30,51,54] (Table S2, ESI†). Both Dy(III) atoms are non-acoordinated but their respective coordination spheres as to the composition are different with O$_7$N$_2$ and O$_8$N donor sets; three chelating nitrate ligands contribute to the coordination of the respective Dy(III) atoms, one is coordinated to Dy1 and two to the Dy2 atom (Fig. 1a). Results of the SHAPE calculations[55] indicate that the coordination polyhedra around the respective Dy(III) atoms can be best described as spherical tricapped trigonal prisms (Fig. 2, Table S3, ESI†). The Dy–O and Dy–N bonds are in the range 2.293(2)–2.634(4) and 2.480(5)–2.537(5) Å, respectively and these values are longer in comparison with the one measured at 186 K (2.287–2.608 and 2.468–2.533 Å), as expected.

The neighbouring dinuclear dysprosium molecules are interconnected by O–H···O type hydrogen bonds in which nitrato ligands and solvate methanol molecules are involved (Fig. 3 and Table S4, ESI†). These hydrogen bonds lead to the formation of a supramolecular chain-like arrangement of the dinuclear molecules (Fig. 3). The packing view along the *c* axis shows that the packing of the dinuclear complex molecules leads to the formation of channels running along the *c* axis and
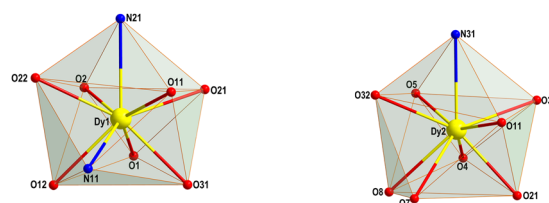

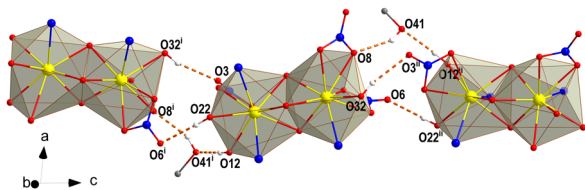**Fig. 2** View of the coordination polyhedra of the respective Dy(III) atoms in **1**.

Fig. 3 View of the hydrogen bonding system in **1**. For the sake of clarity, carbon atoms and hydrogen atoms not involved in hydrogen bond formation are omitted. Dy(ɪɪɪ) atoms are yellow balls while nitrogen atoms are blue balls. Symmetry codes: i: $1/3 − x + y$, $2/3 − x$, $−1/3 + z$; ii: $2/3 − y$, $1/3 + x − y$, $1/3 + z$.

these channels are occupied by additional solvent methanol molecules (Fig. 4). The packing view along the *a* axis is shown on Fig. S2 (ESI†). These highly disordered methanol solvent molecules in the canals are rather isolated from other atoms in the structure as no non-covalent contacts up to 4 Å were found.

DC magnetic data

The Dy(ɪɪɪ) centre in its ground state (multiplet) $^6H_{15/2}$ possesses $L = 5$, $S = 5/2$, and $J = L + S = 15/2$. The product function then adopts a value of $\chi T/C_0 = 37.78$ (dimensionless, $C_0 = N_A\mu_0\mu_B^2/k_B$ is the reduced Curie constant containing only fundamental physical constants in their usual meaning); for two centres it is 75.6. The value observed at room temperature is $\chi T/C_0 = 68.9$ and it decreases on cooling to 27.3 at $T = 2.0$ K. The temperature dependence of the effective magnetic moment is shown in Fig. 5. Its room temperature value is $\mu_{eff}/\mu_B = 14.4$ and it drops to 9.1 at $T = 2.0$ K. The magnetization per formula unit at $T = 2.0$ K and $B = 7$ T approaches the value of $M_1 = M_{mol}/N_A\mu_B = 11.5$ (Fig. 5, right).

A simple coupling scheme for dinuclear species utilized the Hamiltonian that involves the isotropic exchange coupling constant J_{ex}, the anisotropic *g*-factors (g_z, g_x), and partially the crystal-field effects *via* the Stevens operators B_0^2 and B_2^2

$$\hat{H}_a = -J_{ex}(\vec{J}_1 \cdot \vec{J}_2)\hbar^{-2} + \mu_B B g_a(\hat{J}_{z1} + \hat{J}_{z2})\hbar^{-1} \\ + B_0^2(\hat{J}_{z1}^2 - \vec{J}_1^2/3) + B_0^2(\hat{J}_{z2}^2 - \vec{J}_2^2/3)\hbar^{-2} \tag{1}$$
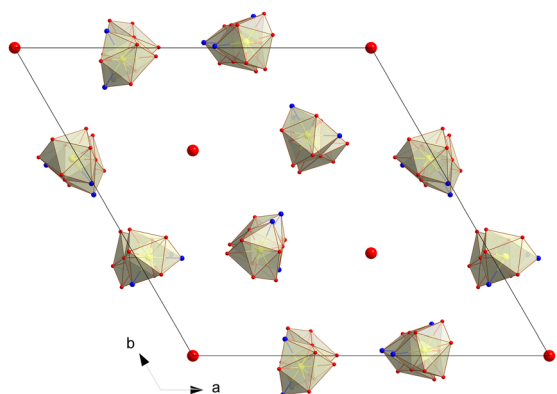

Fig. 4 View of the packing of the structure of **1** along the *c* axis. Only the shared polyhedra around the Dy(ɪɪɪ) central atoms are shown for clarity. The large red balls represent the positions of the methanol solvate molecules in the channels between the complex molecules.
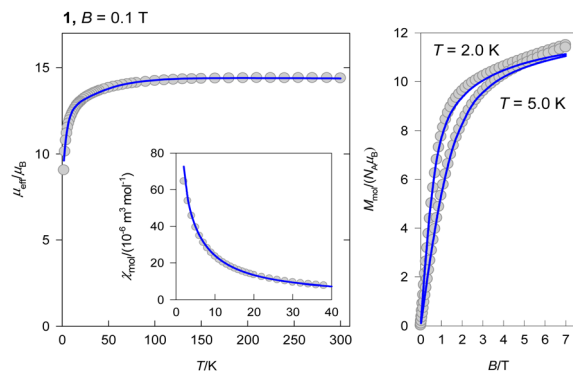

Fig. 5 DC magnetic data for **1**. Solid lines – fitted with the exchange coupling model (left). Field dependence of the magnetization per formula unit (right).

($a = z$, x) with constituent angular momenta $J = 15/2$ and the corresponding operators. The fitting procedure gave $J_{ex}/hc = −0.007(2)$ cm^{-1}, $B_0^2/hc = 5(3)$ cm^{-1}, $B_2^2 \sim 0$, $g_z = 1.3(6)$ and $g_x = 1.2(1)$ (close to the theoretical value of $g_J = 4/3$). Such a small value of the exchange coupling constant means that the maximum at the susceptibility *vs* temperature curve is not seen (it lies below 2 K). Notice, the angles Dy–O–Dy = 96 deg are close to the border when the antiferromagnetic coupling switches to the ferromagnetic one.[4]

AC susceptibility data

The AC susceptibility data for **1** are displayed in Fig. 6. This system shows slow magnetic relaxation even in the absence of an external magnetic field. The field dependence of the out-of-phase susceptibility for individual frequencies *f* of the AC field shows two peaks confirming that there are two relaxation channels: the low-frequency LF, and the high-frequency HF. However, the maximum of the HF peak lies above the hardware limit ($f > 1500$ Hz). With increasing external magnetic field, the HF peak tends to be suppressed and the LF peak bears significance.

The in-phase and out-of-phase susceptibility were fitted simultaneously by employing the two-set Debye model and minimizing the combined functional based upon relative errors of two data sets: $F = E(\chi') \times E(\chi'')$ – see ESI.† This model consists of seven free parameters: a pair of isothermal susceptibilities χ_{T1} and χ_{T2}, two distribution parameters α_1 and α_2, and two relaxation times τ_1 and τ_2 along with the common adiabatic susceptibility χ_S. The low-frequency channel is strongly supported by the external magnetic field. At $T = 2.0$ and $B_{DC} = 0.1$, 0.2, 0.3, 0.4 and 0.5 T, the mole fraction of the low-frequency species rises as $x_{LF} = 0.02$, 0.06, 0.43, 0.46 and 0.48, respectively; along this series the relaxation time is $\tau_{LF} = 21(8)$, 49(7), 48(4), 51(3) and 57(2) ms, respectively. Because of the limited amount of HF data, the parameters for the HF channel suffer from large standard deviations. Therefore, the temperature effect giving rise to the Arrhenius-like plot $\ln\tau_{HF}$ *vs.* T^{-1} has not been studied. The problem unresolved so far is that there is a lack of any theory concerning the nature of the low-frequency
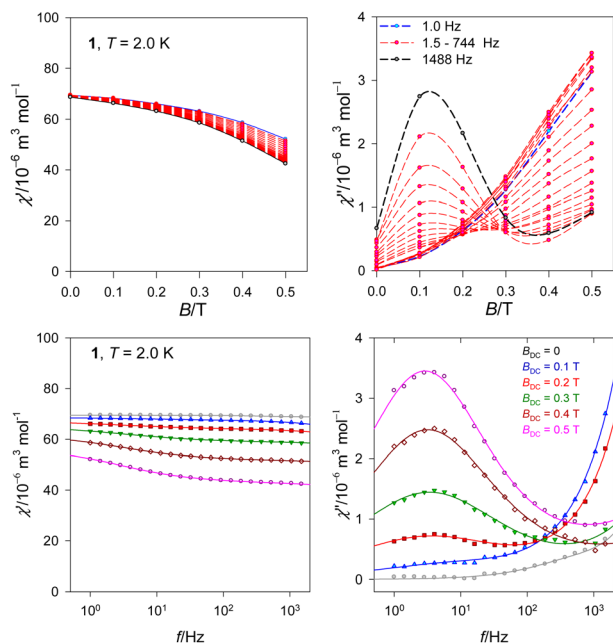
Fig. 6 Field dependence (top) and frequency dependence (bottom) of the AC susceptibility components [SI units] for **1** at T = 2.0 K. Full lines – fitted, dashed – guide for the eyes.

channel in AC susceptibility data. All existing theories refer to the "standard" situation for the single frequency or high-frequency relaxation channels.

Conclusions

In-situ condensation reaction of $Dy(NO_3)_3 \cdot 6H_2O$ with salicylaldehyde and 1-amino-2-propanol in the presence of triethylamine in methanol generated a nine-coordinated dinuclear complex $[Dy_2(NO_3)_3(L)_3] \cdot nCH_3OH$ (n = 1.20) with a $\{Dy_2O_3\}$ core and short $Dy \cdots Dy$ distance of 3.4552(2) Å (**1**). The magnetic property studies of **1** in the 2.0–300 K range revealed weak antiferromagnetic interactions. AC susceptibility studies of **1** show slow magnetic relaxation even in zero field. The low-frequency relaxation channel is strongly supported by the external magnetic field. At B_{DC} = 0.5 T and T = 2.0 the mole fraction of the low-frequency species is x_{LF} = 0.48 and the relaxation time is τ_{LF} = 57 ms.

Author contributions

Mamo Gebrezgiabher: design, synthesis of the chemical compound, conceptualization, methodology, molecular spectroscopy study and analysis, formal analysis, investigation, writing – original draft of the article, writing – review & editing, visualization. Sören Schlittenhardt: magnetic characterization, formal analysis, investigation, data curation, visualization, writing – review & editing, visualization. Cyril Rajnák: supervision, DC and AC magnetism studies and analysis, theoretical studies, magneto-structural correlations, funding acquisition, formal analysis, investigation, resources, data curation, writing – review

& editing, visualization. Juraj Kuchár: crystallographic studies, SHAPE symmetry studies, formal analysis, investigation, data curation, writing – review & editing, visualization. Assefa Sergawie: supervision, editing, writing – review & editing, visualization. Juraj Černák: crystallographic studies, SHAPE symmetry studies, formal analysis, investigation, data curation, writing – review & editing, visualization. Mario Ruben: magnetic characterization, supervision, editing, and reviewing, data curation, writing – review & editing, visualization. Madhu Thomas: supervision, editing, formal analysis, investigation, data curation, writing – review & editing, visualization. Roman Boča: supervision, DC and AC magnetism studies and analysis, theoretical studies, magnetic data fitting, funding acquisition, formal analysis, investigation, resources, data curation, writing – review & editing, visualization.

Conflicts of interest

There are no conflicts to declare.

Acknowledgements

References

1 D. N. Woodruff, R. E. P. Winpenny and R. A. Layfield, *Chem. Rev.*, 2013, **113**, 5110–5148.

2 J. L. Liu, Y. C. Chen and M. L. Tong, *Chem. Soc. Rev.*, 2018, **47**, 2431–2453.

3 L. Bogani and W. Wernsdorfer, *Nat. Mater.*, 2008, **7**, 194–201.

4 O. Kahn, *Molecular Magnetism*, VCH Pubilshers, New York, 1993.

5 R. Sessoli, D. Gatteschi, A. Caneschi and M. A. Novak, *Nature*, 1993, **365**, 141–143.

6 S. K. Langley, N. F. Chilton, B. Moubaraki and K. S. Murray, *Dalton Trans.*, 2012, **41**, 1033–1046.

7 P. Abbasi, K. Quinn, D. I. Alexandropoulos, M. Damjanovi, A. Escuer, J. Mayans, M. Pilkington and T. C. Stamatatos, *J. Am. Chem. Soc.*, 2017, **139**, 15644–15647.

8 A. M. Ako, I. J. Hewitt, V. Mereacre, R. Clérac, W. Wernsdorfer, C. E. Anson and A. K. Powell, *Angew. Chem., Int. Ed.*, 2006, **45**, 4926–4929.

9 K. S. Gavrilenko, O. Cador, K. Bernot, P. Rosa, R. Sessoli, S. Golhen, V. V. Pavlishchuk and L. Ouahab, *Chem. – Eur. J.*, 2008, **14**, 2034–2043.

10 A. Kawamura, A. S. Filatov, J. S. Anderson and I. Jeon, *Inorg. Chem.*, 2019, **58**, 3764–3773.

11 G. Wu, R. Clérac, W. Wernsdorfer, S. Qiu, C. E. Anson, I. J. Hewitt and A. K. Powell, *Eur. J. Inorg. Chem.*, 2006, 1927–1930.

12 N. Portolés-Gil, S. Gómez-Coca, O. Vallcorba, G. Marbán, N. Aliaga-Alcalde, A. López-Periago, J. A. Ayllón and C. Domingo, *RSC Adv.*, 2020, **10**, 45090–45104.

13 R. Clérac, H. Miyasaka, M. Yamashita and C. Coulon, *J. Am. Chem. Soc.*, 2002, **124**, 12837–12844.

14 H. Oshio, M. Nihei, S. Koizumi, T. Shiga, H. Nojiri, M. Nakano, N. Shirakawa and M. Akatsu, *J. Am. Chem. Soc.*, 2005, **127**, 4568–4569.

15 V. Mereacre, A. M. Ako, R. Clérac, W. Wernsdorfer, I. J. Hewitt, C. E. Anson and A. K. Powell, *Chem. – Eur. J.*, 2008, **14**, 3577–3584.

16 M. Dolai, M. Ali, C. Rajnák, J. Titiš and R. Boča, *New J. Chem.*, 2019, **43**, 12698–12701.

17 S. Hazra, J. Titiš, D. Valigura, R. Boča and S. Mohanta, *Dalton Trans.*, 2016, **45**, 7510–7520.

18 A. Vráblová, M. Tomás, L. R. Falvello, Ľ. Dlháň, J. Titiš, J. Černák and R. Boča, *Dalton Trans.*, 2019, **48**, 13943–13952.

19 Y. N. Guo, G. F. Xu, Y. Guo and J. Tang, *Dalton Trans.*, 2011, **40**, 9953–9963.

20 S. T. Liddle and J. van Slageren, *Chem. Soc. Rev.*, 2015, 6655–6669.

21 R. Vincent, S. Klyatskaya, M. Ruben, W. Wernsdorfer and F. Balestro, *Nature*, 2012, **488**, 357–360.

22 S. Loth, S. Baumann, C. P. Lutz, D. M. Eigler and A. J. Heinrich, *Science*, 2012, **335**, 196–200.

23 A. Ardavan, O. Rival, J. J. L. Morton, S. J. Blundell, A. M. Tyryshkin, G. A. Timco and R. E. P. Winpenny, *Phys. Rev. Lett.*, 2007, **98**, 1–4.

24 J. Tang, I. Hewitt, N. T. Madhu, G. Chastanet, W. Wernsdorfer, C. E. Anson, C. Benelli, R. Sessoli and A. K. Powell, *Angew. Chem., Int. Ed.*, 2006, **45**, 1729–1733.

25 J. D. Rinehart and J. R. Long, *Chem. Sci.*, 2011, **2**, 2078–2085.

26 A. Bhunia, M. T. Gamer, L. Ungur, L. F. Chibotaru, A. K. Powell, Y. Lan, P. W. Roesky, F. Menges, C. Riehn and G. Niedner-Schatteburg, *Inorg. Chem.*, 2012, **51**, 9589–9597.

27 S. Mukherjee, J. Lu, G. Velmurugan, S. Singh, G. Rajaraman, J. Tang and S. K. Ghosh, *Inorg. Chem.*, 2016, **55**, 11283–11298.

28 S. Mukherjee, A. K. Chaudhari, S. Xue, J. Tang and S. K. Ghosh, *Inorg. Chim. Acta*, 2013, **35**, 144–148.

29 R. Boča, M. Stolárová, L. R. Falvello, M. Tomás, J. Titiš and J. Černák, *Dalton Trans.*, 2017, **46**, 5344–5351.

30 J. Long, F. Habib, P. H. Lin, I. Korobkov, G. Enright, L. Ungur, W. Wernsdorfer, L. F. Chibotaru and M. Murugesu, *J. Am. Chem. Soc.*, 2011, **133**, 5319–5328.

31 M. Gebrezgiabher, Y. Bayeh, T. Gebretsadik, G. Gebreslassie, F. Elemo, M. Thomas and W. Linert, *Inorganics*, 2020, **8**, 1–66.

32 Y. Guo, G. Xu, P. Gamez, L. Zhao, S. Lin, R. Deng, J. Tang and H.-J. Zang, *J. Am. Chem. Soc.*, 2010, **132**, 8538–8539.

33 Y. N. Guo, G. F. Xu, Y. Guo and J. Tang, *Dalton Trans.*, 2011, **40**, 9953–9963.

34 Y. X. Zhang, X. Y. Cheng, Y. T. Tang, Y. H. Zhang, S. C. Wang, H. Y. Wei and Z. L. Wu, *Polyhedron*, 2019, **166**, 23–27.

35 Y. Guo, X. Chen, S. Xue and J. Tang, *Inorg. Chem.*, 2012, **51**, 4035–4042.

36 K. Liu, W. Shi and P. Cheng, *Coord. Chem. Rev.*, 2015, **289–290**, 74–122.

37 A. Khan, O. Fuhr, M. N. Akhtar, Y. Lan, M. Thomas and A. K. Powell, *J. Coord. Chem.*, 2020, **73**, 1–10.

38 J. D. Rinehart, M. Fang, W. J. Evans and J. R. Long, *Nat. Chem.*, 2011, **3**, 538–542.

39 R. J. Blagg, C. A. Muryn, E. J. L. McInnes, F. Tuna and R. E. P. Winpenny, *Angew. Chem.*, 2011, **123**, 6660–6663.

40 Y. N. Guo, X. H. Chen, S. Xue and J. Tang, *Inorg. Chem.*, 2011, **50**, 9705–9713.

41 P. Zhang, L. Zhang, S. Lin, S. Xue and J. Tang, *Inorg. Chem.*, 2013, **52**, 4587–4592.

42 K. Senthil Kumar, Y. Bayeh, T. Gebretsadik, F. Elemo, M. Gebrezgiabher, M. Thomas and M. Ruben, *Dalton Trans.*, 2019, **48**, 15321–15337.

43 M. Gebrezgiabher, S. Schlittenhardt, C. Rajnák, A. Sergawie, M. Ruben, M. Thomas and R. Boča, *Inorganics*, 2022, **10**, 66.

44 J. Long, F. Habib, P. H. Lin, I. Korobkov, G. Enright, L. Ungur, W. Wernsdorfer, L. F. Chibotaru and M. Murugesu, *J. Am. Chem. Soc.*, 2011, **133**, 5319–5328.

45 R. CrysAlisPro 1.171.41.93a, Oxford Diffraction, Oxford Diffraction Ltd, England, 2020.

46 G. M. Sheldrick, *Acta Crystallogr., Sect. A: Found. Crystallogr.*, 2015, **71**, 3–8.

47 G. M. Sheldrick, *Acta Crystallogr., Sect. C: Struct. Chem.*, 2015, **71**, 3–8.

48 G. M. S. Sheldrick, *Crystal structure refinement with SHELXL*, Bruker AXS Inc, Madison, WI, WI, vol. version 5, 1997.

49 L. J. Farrugia, *J. Appl. Crystallogr.*, 2012, **45**, 849–854.

50 Diamond - Crystal and Molecular Structure Visualization, Crystal Impact – Dr H. Putz & Dr K. Brandenburg GbR, Kreuzherrenstr. 102, 53227 Bonn, Germany., 2022.

51 L. Zhang, Y. Ji, X. Xu, Z. Liu and J. Tang, *J. Lumin.*, 2012, **132**, 1906–1909.

52 Kazuo Nakamoto, *Infrared and Raman Spectra of Inorganic and Coordination Compounds Part A: Theory and Applications in Inorganic Chemistry*, John Wiley & Sons, Inc., Hoboken, New Jersey, 2008.

53 E. Moreno Pineda, N. F. Chilton, R. Marx, M. Dörfel, D. O. Sells, P. Neugebauer, S. Da Jiang, D. Collison, J. Van Slageren, E. J. L. McInnes and R. E. P. Winpenny, *Nat. Commun.*, 2014, **5**, 1–7.

54 D. Aguilà, L. A. Barrios, F. Luis, A. Repollés, O. Roubeau, S. J. Teat and G. Aromí, *Inorg. Chem.*, 2010, **49**, 6784–6786.

55 M. Llunell, D. Casanova, J. Cirera, P. Alemany and S. Alvarez, SHAPE - Program for the Stereochemical Analysis of Molecular Fragments by Means of Continuous Shape Measures and Associated Tools, Version 2.1, University of Barcelona, Spain, 2013.